Advantages of Switched Reluctance Motor Applications to EV and HEV: Design and Control Issues

Khwaja M. Rahman, *Student Member, IEEE*, Babak Fahimi, *Student Member, IEEE*, G. Suresh, *Student Member, IEEE*, Anandan Velayutham Rajarathnam, *Student Member, IEEE*, and M. Ehsani, *Fellow, IEEE*

***Abstract*—Land vehicles need their drivetrain to operate entirely in constant power in order to meet their operational constraints, such as initial acceleration and gradability, with minimum power rating. The internal combustion engine (ICE) is inappropriate for producing this torque–speed profile. Therefore, multiple gear transmission is necessary with the ICE in a vehicle. Some electric machines, if designed and controlled appropriately, are capable of producing an extended constant power range. The purpose of this paper is to investigate the capabilities of the switched reluctance motor (SRM) for electric vehicle and hybrid electric vehicle applications. This investigation will be carried out in two steps. The first step involves the machine design and the finite-element analysis to obtain the static characteristic of the motor. In the second step, the finite-element field solutions are used in the development of a nonlinear model to investigate the dynamic performance of the designed motor. Several 8-6 and 6-4 SRM geometries will be investigated. Effects of different stator and rotor pole widths and pole heights on the steady state as well as on the dynamic performance of the motor will be studied. The air gap for each motor will be made as small as manufacturally possible. The aspects of performance to be compared for each design motor are: 1) the range of the constant power operation; 2) drive efficiency in this extended constant power range; 3) the power factor in this operational range; and 4) the short time overload capability. The first performance index defines the rated power of the motor. The longer the constant power range, the lower is the power rating for the same vehicle performance. Hence, special emphasis will be given to this. In the high-speed operation of the SRM, there will be considerable phase overlapping. Hence, thicker back iron than usual might be needed to prevent the back iron from saturating. However, since flux peaking of each phase occurs at different rotor positions, the phase overlapping might not necessitate special designing of the back iron. However, the possibility of the back iron being saturated will not be neglected and will be investigated. The optimal control parameters of the SRM, which maximize the constant power range with maximum torque per ampere, will be calculated. A performance comparison will be made for this optimal operation. Simulation results of the designed SRM will be presented for vehicle acceleration. To demonstrate the capability of the SRM in producing an extended constant power range, experimental results will be presented, however, for a reduced size motor available commercially.**

***Index Terms*—Constant power range, electric vehicle, hybrid electric vehicle, switched reluctance motor drive.**

I. Introduction

THE switched reluctance motor (SRM) is gaining much interest as a candidate for electric vehicle (EV) and hybrid electric vehicle (HEV) electric propulsion for its simple and rugged construction, ability of extremely high-speed operation, and hazard-free operation. In view of these characteristics, one of the early SRM's was designed and built for EV application [1]. In designing this SRM, the major attention was given to the efficiency of the drive. Later, an optimized design method of an SRM was reported in [2] for EV application. The design optimization was based on a static analytical model of an SRM, similar to the one developed by Corda and Stephenson [3]. Moreover, the efficiency optimization was carried out for the constant-speed operation of the drive with nonoptimal control. Like the previous design, the special emphasis was given in this design to the drive efficiency and, additionally, to the drive cost. Most recently, a 100-hp SRM was designed and built in [4] for EV application. No special control scheme, design method, or optimization technique were, however, presented.

While designing an SRM in all the previous methods, no attention was given to the vehicle dynamics. Vehicle dynamics dictate a special torque–speed profile for its propulsion system. Our recent study has shown that, a vehicle, in order to meet its operational constraints, such as initial acceleration and gradability with minimum power, needs the power train to operate entirely in constant power [5]. The power rating of a motor that deviates from the constant-power regime can be as much as two times that of a motor operating at constant power throughout its speed range in a vehicle. Operation entirely in constant power is not possible for any practical drive. An extended constant power range is, however, possible if the motor is appropriately designed and its control strategy is properly selected.

This paper will investigate the capabilities of the SRM for vehicle traction. For this purpose, several SRM's will be designed and their optimal control parameters, which maximize the constant horse power range, will be calculated. A two–dimensional (2-D) finite-element analysis will be used to obtain

Paper IPCSD 99–11, presented at the 1998 Industry Applications Society Annual Meeting, St. Louis, MO, October 12–16, and approved for publication in the IEEE TRANSACTIONS ON INDUSTRY APPLICATIONS by the Electric Machines Committee of the IEEE Industry Applications Society. Manuscript submitted for review July 24, 1998 and released for publication July 23, 1999. This work was supported by the Texas Higher Education Coordinating Board Advanced Technology Program, the Texas Transportation Institute, and the Texas Instrument Digital Control Systems Division.

K. W. Rahman was with the Department of Electrical Engineering, Texas A&M University, College Station, TX 77843-3128 USA. He is now with General Motors, Advanced Technology Vehicle, Torrance, CA 90509-2923 USA (e-mail: rahmank@pcssmtp.hac.com).

B. Fahimi, G. Suresh, A. V. Rajarathnam, and M. Ehsani are with the Department of Electrical Engineering, Texas A&M University, College Station, TX 77843-3128 USA (e-mail: fahimi@ee.tamu.edu; suresh@ee.tamu.edu; rajarath@ee.tamu.edu; ehsani@ee.tamu.edu).

Publisher Item Identifier S 0093-9994(00)00037-2.

the static characteristics of designed motors. The finite-element field solutions will then be used in the development of a nonlinear model to investigate the steady-state and the dynamic performance of the designed motors. The nonlinear model will also be used to search for the optimal control parameters (turn-on and turn-off angles) of each designed SRM which extends the constant power range with maximum torque per ampere. A performance comparison will be made for this optimal operation. Several 8-6 and 6-4 SRM geometries will be investigated. Effects of different stator and rotor pole geometries on the steady— state as well as on the dynamic performance of the motor will be studied. In the high-speed operation of the SRM, there will be considerable phase overlapping. Hence, thicker back iron than normal might be needed to prevent it from saturating. However, since flux peaking of each phase occurs at different rotor positions, the phase overlapping might not bring the back iron into saturation. However, the possibility of back iron being saturated will not be neglected and will be investigated. Besides the range of the constant power operation, the other aspects of performance which will be investigated for each designed motor are: 1) the drive efficiency in this extended constant power range; 2) the power factor (PF) in this operational range; and 3) the short time overload capability. Simulation results of each designed SRM in vehicle acceleration will be presented. To demonstrate that the SRM is capable of producing a long constant-power range when controlled optimally, experimental results will also be presented, however, for a reduced size motor available commercially.

II. SRM Static Characteristics

To investigate the dynamic and steady-state performance of each SRM geometry considered in this paper, the static torque and flux-linkage characteristics as functions of stator current and rotor position are required. The nonlinearity of the SRM owing to its saturation region of operation, however, complicates the analysis. Several nonlinear analytic models of SRM are presented in the literature to obtain the static data [3], [6]–[8]. For accuracy, we will, however, rely on the finite-element analysis to obtain the static data. Finite-element analysis will be performed on several 6-4 and 8-6 SRM geometries with varying stator and rotor pole widths and heights. Later, the static torque and flux-linkage data obtained from the finite-element analysis will be used in the dynamic model to determine the drive performance with optimal control parameters.

III. Nonlinear SRM Model

A block diagram of the nonlinear SRM model is shown in Fig. 1. The static flux-linkage and torque data as functions of the stator current and rotor position, obtained from the finite-element analysis for each SRM geometry, are used in the dynamic model in order to include the effect of magnetic nonlinearity. This model is used to predict the drive performance at steady state and in the dynamics. The optimal control parameters are obtained by using the dynamic model. A linear model of the converter is used in the dynamic model. The semiconductor switch and diode parameters used in the dynamic model are obtained from the manufacturer's provided data. The core loss model presented in [15] is used with the SRM nonlinear model to predict the core losses of each designed SRM.

IV. Determination of the Optimal Control Parameters

Base speed in any motor is defined as the speed at which the back EMF equals the bus voltage. The motor also reaches its rated power at this speed for rated excitation (current). Torque in an SRM below base speed, when the back EMF is lower than the bus voltage is controlled, like all other motors, by the pulsewidth modulation (PWM) control of current. Above base speed, due to the high back EMF which cannot be field weakened, PWM control of current is not possible. Operation in constant power is made possible in this motor by the phase advancing of the stator phase current until overlapping between the successive phases occurs [9]. Torque control below base speed can be optimized by the stator current profiling [10], [11]. However, above base speed, the only control parameters are the phase turn-on and the turn-off angles. The phase turn-on and the turn-off angles can be optimally controlled above base speed to maximize the range of the constant power operation with maximum torque per ampere. To find the optimal turn-on and the turn-off angles, the dynamic model developed in the earlier section is used. The search procedure for the optimal angles is lengthy and time consuming. Any standard root-seeking methods, such as the Secant method [12], may be used to accelerate the speed of the searching process. After a series of iterations, the dynamic model finds the optimal turn-on and turn-off angles. To implement the control scheme in real time, a neural-network-based controller may be implemented [10].

V. Design Methodology

The design process starts with the hand calculation of several SRM geometries with varying pole numbers and pole dimensions. A 2-D finite- element analysis is then performed to obtain the nonlinear field solutions within the motor. The finite-element field solutions are used in the development of a nonlinear SRM model. The developed model is used to search the optimal control parameters which extends the constant power range of each motor with maximum torque per ampere. Both the steady-state and the dynamic performance of each designed SRM are investigated for these optimal control parameters. These steps are repeated for each designed SRM in an attempt to determine an appropriate SRM geometry for EV and HEV applications. In this paper, we will consider only the 8-6 and 6-4 SRM geometries. SRM geometries with more stator and rotor poles will have less space for phase advancing. As a consequence, the motor will suffer from limited constant-power range. Moreover, the ratio of the aligned to unaligned inductance will reduce with increased number of rotor and stator poles. This will reduce the static torque and increase the converter voltamperes [9].

VI. Design Examples

In this section, we will present several SRM designs and will investigate their performance when controlled optimally. Our goal is to extend the constant-power range with maximum torque per ampere. Special attention will also be given to the

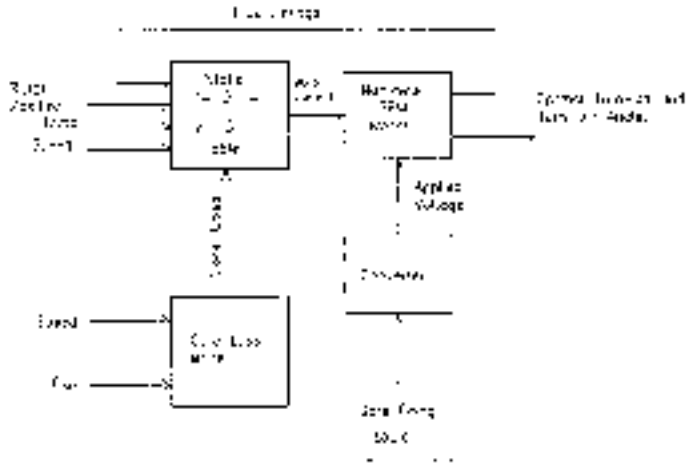

Fig. 1. A block diagram of the dynamic SRM model.

drive efficiency. All the design examples considered in this paper have almost the same stator outer dimension and stack length. We begin with the 6-4 SRM designs.

A. 6-4 SRM Design

First, we will examine the effect of the pole widths on the SRM performance. The minimum stator and rotor pole widths of a 6-4 SRM should be 30° in order to have adequate starting torque from all positions. To maximize the room available for winding placement, we will keep the stator pole width fixed at 30°, while the rotor pole widths will be varied. The considered SRM's have the following dimensions:

- stator outer diameter, 13.58 in;
- rotor outer diameter, 7.4694 in;
- stack length, 7.4694 in;
- air gap, 0.0373 in;
- stator slot height, 1.7166 in;
- rotor slot height, 0.9763 in;
- stator core thickness, 1.3017 in;
- rotor core thickness, 1.3517 in;
- M19 steel;
- shaft diameter, 2.8135 in;
- number of turns per pole, 14;
- dc-bus voltage, 240 V;
- rated phase current, 168.3 A (air cooled, 4 A/mm^2);
- stator pole arc, 30°;
- rotor pole arcs, 30.31 (same pole width as the stator), 31.5°, 34°, and 36°.

The dimensions of the four SRM's are the same except for the rotor pole arc, which varies from 30.31° (same as the stator pole width) to 36°. For convenience, we will label these designs as designs 1–4. Finite-element analysis is performed on each of these motors in order to obtain the nonlinear field solutions. These field solutions are then used in the nonlinear model to determine the steady-state and the dynamic performance of each of the designed SRM's. Fig. 2(a) shows the constant-power ranges of these motors. The optimal turn-on and the turn-off angles and the phase rms currents for the constant power operation of Fig. 2(a) are shown in Fig. 2(b). Extended speed constant-power

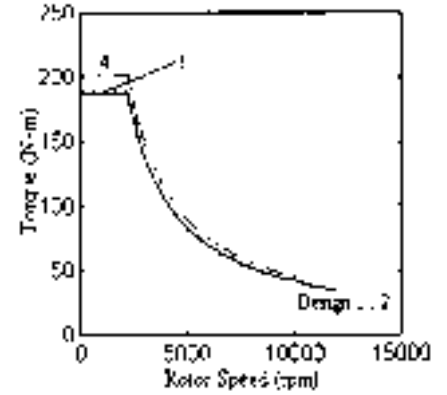

(a)

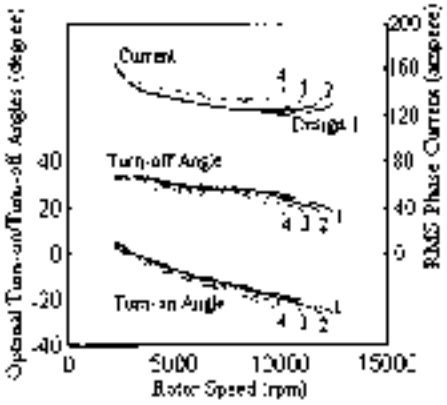

(b)

Fig. 2. (a) Extended constant power range and (b) optimal control angles and rms phase current for SRM designs 1–4.

ranges are obtained for these designs when controlled with the optimal parameters. The extended constant-power range is maximum (5.7 times the base speed) for design 1 (narrowest rotor pole), while it is minimum (4.7 times the base speed) for design 4 (widest rotor pole). However, the rated torque is minimum for design 1 and maximum for design 4. The long constant-power range available from motor 1 will make it highly favorable for vehicle applications, despite the fact that it has a lower rated torque (power). The vehicle performance analysis for all these motors will be presented later. We can see in Fig. 2(b) that lower than rated rms current is needed at higher speeds to maintain constant power at the output. This is a direct consequence of the fact that the PF of operation of the motors is improving at higher speed. The PF's and the drive efficiencies for these motors are presented in Fig. 3 for the constant-power operation. We have used the following definition for calculating the PF:

$$\text{PF} = \frac{\text{output shaft power}}{\text{input rms voltampere}}. \tag{1}$$

Design 1 exhibits both the best efficiency and the PF among these designs.

Since the rms phase current decreases during high-speed constant-power operation, it should be possible to obtain more than the designed rated powers from these motors at high speed without exceeding the bus voltage and the rated current of each motor. This is shown in Fig. 4. Fig. 4(a) shows the maximum

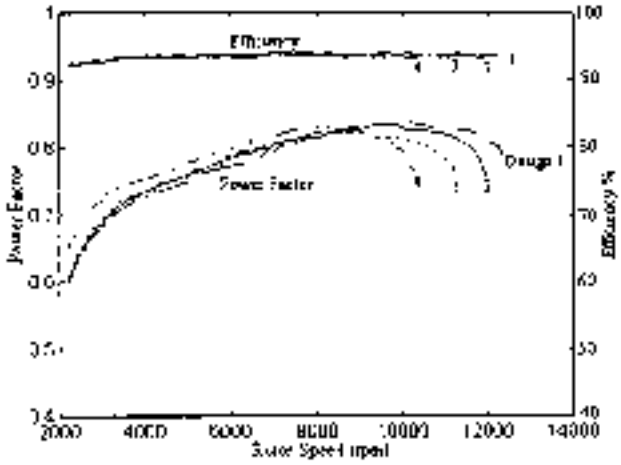

Fig. 3. Efficiency and PF of motors 1–4 for constant power operation.

power available from these motors and Fig. 4(b) shows the phase current and the control angles for the maximum power outputs. The output shaft powers are shown as a ratio of the ideal output power (unity PF) which is only possible from a separately excited dc motor. The power curves shown in Fig. 4 are the maximum powers these motors are capable of delivering, given the voltage and the current limitations. Again, design 1 is exhibiting better performance (higher power) at higher speeds. It may be noted that almost 40% more than the design rated power is obtained. The difference between the ideal power and the actual power is narrowing at the high speed. It is interesting to note that, beyond a certain speed, the rms phase current is reduced from the rated value in order to obtain more power. Any current higher than this will actually reduce the output torque due to the development of more negative torque. Hence, beyond that speed, it is advantageous to reduce the current rather than maintaining the rated current. Motor efficiency and PF for its operation on the maximum power curve of Fig. 4(a) are shown in Fig. 5. Although the rated PF is low for the SRM, this difficulty is greatly overcome at higher speeds and the SRM output power approaches the ideal power (Fig. 4). This will make SRM attractive for applications requiring high-speed operatios, e.g., the vehicle propulsion system.

Vehicle application also requires short-term overload capability from its propulsion system. Hence, finally, we will examine the overload capabilities of these motors. The SRM does not have any breakdown torque like the induction motor. The overload capability, however, would depend on how much current can be pushed in to the motor against the high back EMF and how fast it can be pushed. Obviously, a low unaligned inductance will be favorable for both these conditions. Design 1, which has narrow poles (low unaligned inductance), will have a good overload capability. This is shown in Fig. 6 in per unit of the rated power. As expected, maximum overload capability decreases as the speed increases. Peak overload capability for design 1 at the rated speed is almost 4.5 times its rated power. RMS phase current and optimal control angles are shown in Fig. 6(b). These phase currents for the overload condition may be compared with the currents of Figs. 2 and 4, to understand the

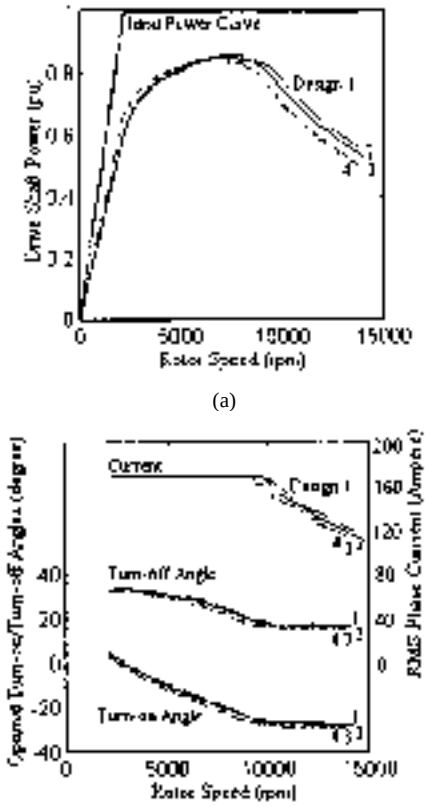

Fig. 4. (a) Maximum output power and (b) optimal control angles and rms phase current for SRM designs 1–4.

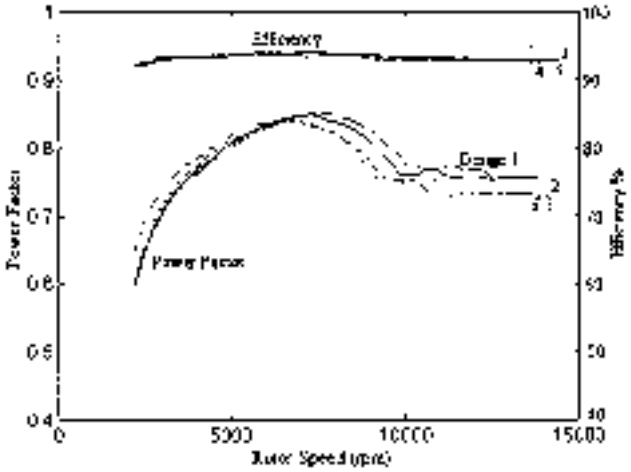

Fig. 5. Efficiency and PF of motors 1–4 for maximum power output.

extent of overload from thermal (cooling requirement) point of view. We would, however, like to point out that the actual overload power would be less than this theoretically predicted overload power. When the motor is severely overloaded, the back iron will saturate. This will introduce strong coupling between phases, which is neglected in the developed model of this paper. Due to these phase couplings, torque and, hence, power will be reduced. Efficiency and PF during motor overloading are shown in Fig. 7.

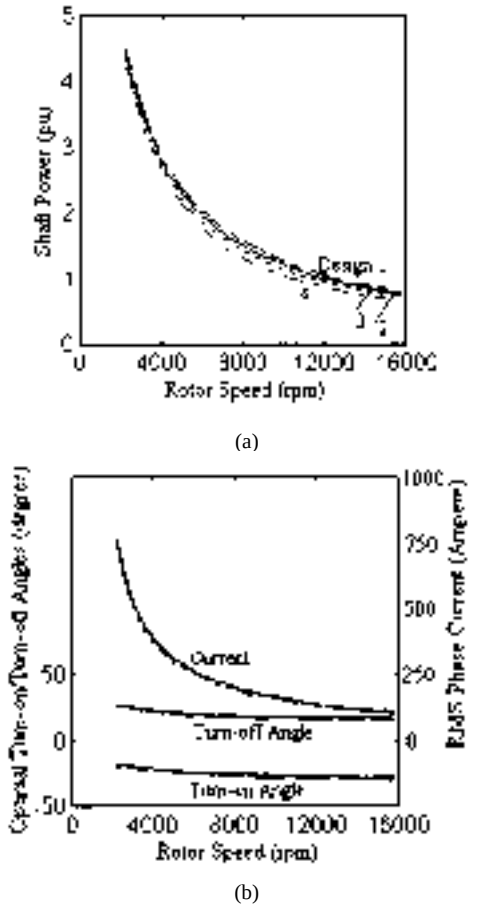

(a)

(b)

Fig. 6 (a) Maximum overload power and (b) rms phase current and optimal angles for SRM designs 1–4.

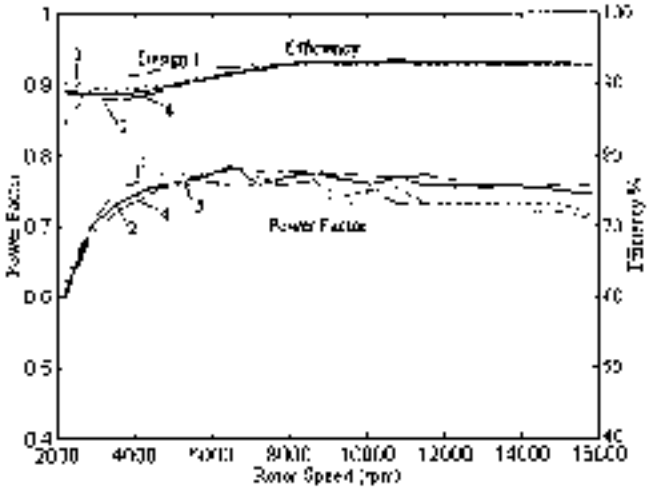

Fig. 7 Efficiency and PF of motors 1–4 during the overloading condition.

Next, we will investigate the effect of rotor pole height on the SRM performance. If the stator outer diameter is fixed, an increase in rotor pole height, however, will decrease the stator slot area. As a consequence, winding area will decrease. Hence, the rated current of the motor will decrease. In the unaligned position, flux also fringes through the side of the rotor pole. Hence, making the rotor pole very long will not be very useful in reducing the unaligned inductance. We will consider four more designs. The rotor pole height of design 2 (rotor pole arc 31.5°) is increased 10% and 20%, and these two designs will be labeled design 5 and 6, respectively. Also, the rotor pole height of design 3 (rotor pole arc 34°) is increased 10 and 20%. These two designs will be labeled design 7 and 8, respectively.

As before, the finite-element analysis is performed on these motors to obtain the field solutions. The nonlinear field solutions are then used in the nonlinear SRM model to examine the drive performance. For better understanding, the performance of designs 5–8 will be presented along with the performance of designs 2 and 3. Fig. 8 shows the constant-power ranges of these motors when controlled optimally. Design 6, which has the narrowest and longest rotor poles among these designs, has the longest constant-power range (7.75 times the base speed), however, the lowest rated torque. On the other hand, design 3, which has the widest and shortest rotor pole, has the highest rated torque, but the shortest constant power range (5.1 times the base speed). The PF and the efficiency of these designs for the constant-power operation are shown in Fig. 9.

The maximum power available from these motors, operating within the voltage and the current limitations, is shown in Fig. 10 and the corresponding efficiencies and PF's are shown in Fig. 11. The overload capabilities of these motors are shown in Fig. 12 and the PF's and the efficiencies are shown in Fig. 13. Design 6 has an overloading capability of almost seven times the rated power.

Among the eight designs we have presented so far, design 6 has the longest constant-power range, however, the lowest power rating, while design 4 has the shortest constant-power range, however, the highest power rating. A valid comparison between these motors, however, should be made in terms of the vehicle performance, which we will make in the next section. We will present two 8-6 SRM designs next.

B. 8-6 SRM Design

We will present two 8-6 SRM designs in this section. These two designs have the following dimensions:

- stator outer diameter, 13.66 in ;
- rotor outer diameter, 7.5156 in ;
- stack length, 7.5156 in;
- air gap, 0.0376 in;
- stator slot height, 1.9303 in;
- rotor slot height, 1.3152 in;
- stator core thickness, 1.1066 in;
- rotor core thickness, 1.1987 in;
- M19 steel;
- shaft diameter, 2.4878 in;
- number of turns per pole, 11;
- dc-bus voltage, 240 V;
- current density 4 A/mm^2 (air cooled);
- stator and rotor pole arcs 21°, 23° (design 9), and 19°, 21° (design 10).

We have labeled the two SRM designs presented in this section as designs 9 and 10. After performing the finite-element analysis, the optimal constant-power ranges are calculated using

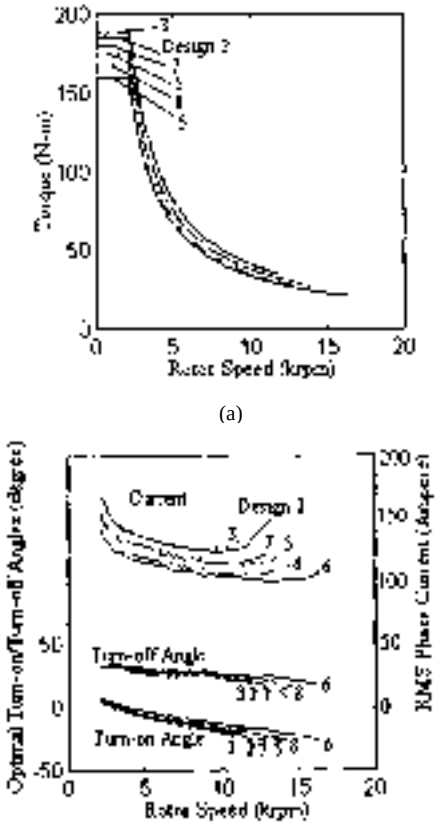

Fig. 8. (a) Extended constant power range and (b) optimal control angles and rms phase current for SRM designs 5–8.

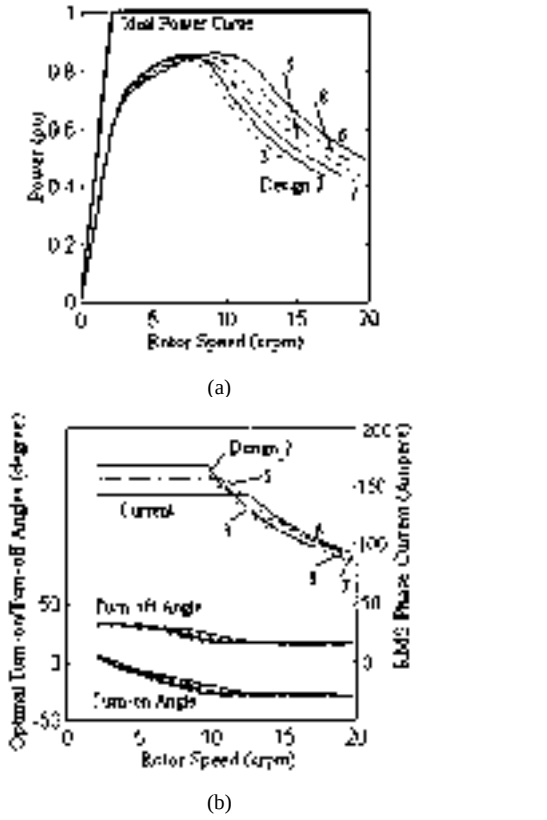

Fig. 10 (a) Maximum output power and (b) optimal control angles and rms phase current for SRM designs 5–8.

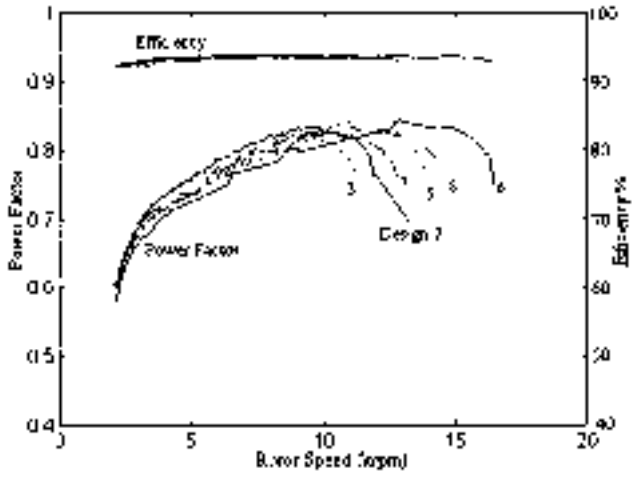

Fig. 9. Efficiency and PF of motors for constant power operation.

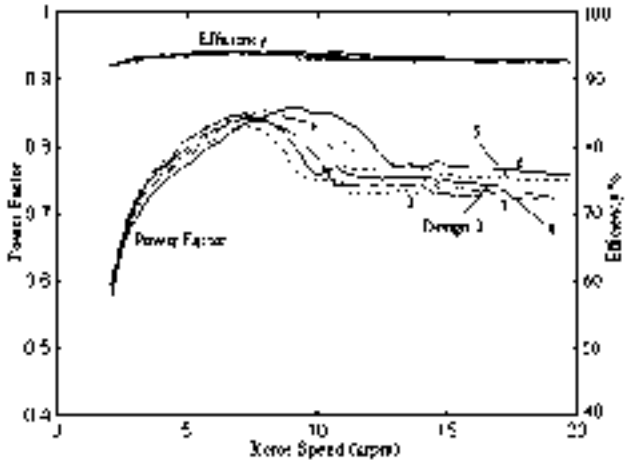

Fig. 11. Efficiency and PF of motors 5–8 for maximum power output.

the dynamic model. Fig. 14 shows the constant-power ranges of these motors along with the rms phase current and the optimal angles. Design 9, which has wider poles, produces higher rated torque, however, a constant power range of only 3.2 times the base speed. Design 10 has slightly lower rated torque and rated power than design 9, but has a much longer constant power range (4.125) than 9. The rms phase current also decreases while maintaining the constant-power operation. The PF and motor efficiency for the constant-power operation are shown in Fig. 15. PF improves considerably in the high-speed constant-power operation of the motors. Design 10 has a lower PF than design 9 at the rated speed, however, it improves rapidly and shows better PF than design 9, roughly after 7000 r/min. The 8-6 designs, although they have shorter constant-power range, are showing better PF and much better power ratings than the 6-4 designs (Figs. 2 and 3). The 8-6 SRM's, due to their pole widths being narrower than the 6-4 SRM's, operate in higher saturation level (6-4 and the 8-6 designs have comparable winding areas). Moreover, the higher phase overlapping in 8-6 motors is contributing more to the average torque. The back iron in 8-6 designs are,

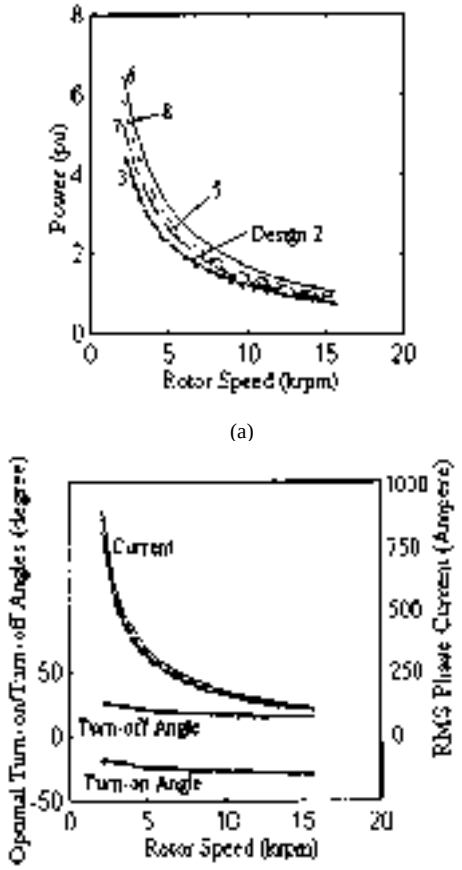

(a)

(b)

Fig. 12. (a) Maximum overload power and (b) rms phase current and optimal angles for SRM designs 5–8.

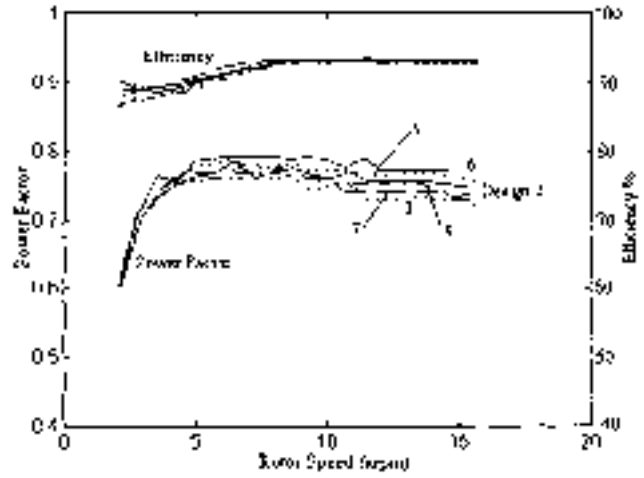

Fig. 13. Efficiency and PF of motors 5–8 during the overloading condition.

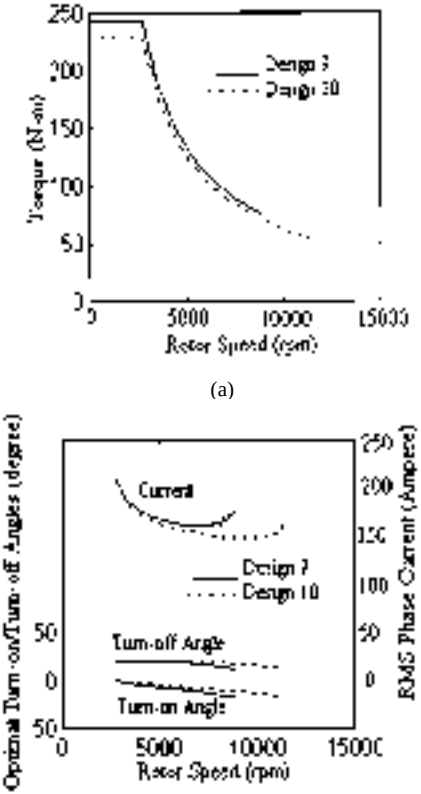

(a)

(b)

Fig. 14. (a) Extended constant power range and (b) optimal control angles and rms phase current for 8-6 SRM designs 9 and 10.

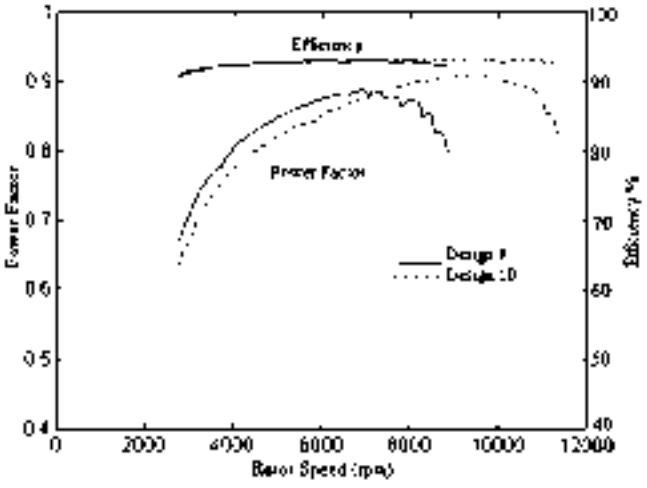

Fig. 15. Efficiency and PF of operation for motors 9 and 10 for their operation on the constant power profile.

however, saturating. The stator and rotor back-iron thickness in both the designs are chosen as 80% of the design 9 respective pole widths. The back irons in both the designs, especially in design 10 (design 10 has higher ampere–turn rating), saturate for the rated torque and near the rated speed of the motor. To prevent this from happening, design 9 would require 6% more core thickness, whereas design 10 would require 20% more core thickness.

Next, we will examine the maximum power capability operating within the rated voltage and current of the motors. Fig. 16 shows the maximum power capability of these two motors in per unit of their ideal output power. Design 10 has higher and wider power capability at high speeds. This is obviously desirable for EV and HEV applications. Efficiency and PF for this operation are shown in Fig. 17. Design 10 is also showing higher PF and efficiency at higher speeds.

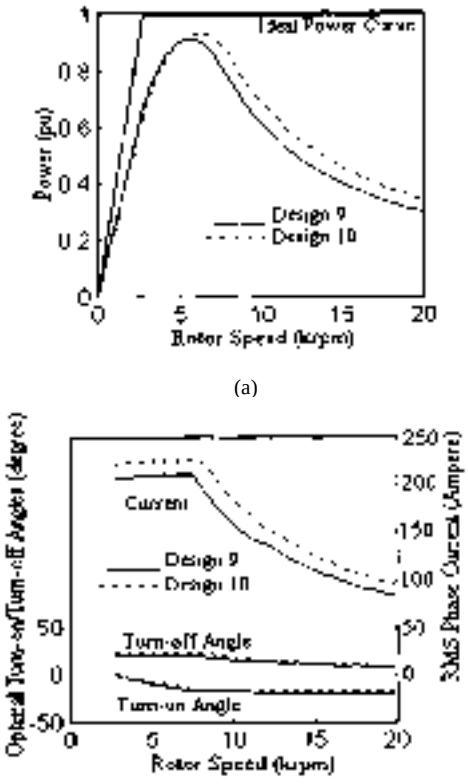

Fig. 16. (a) Maximum output power and (b) optimal control angles and rms phase current for SRM designs 9 and 10.

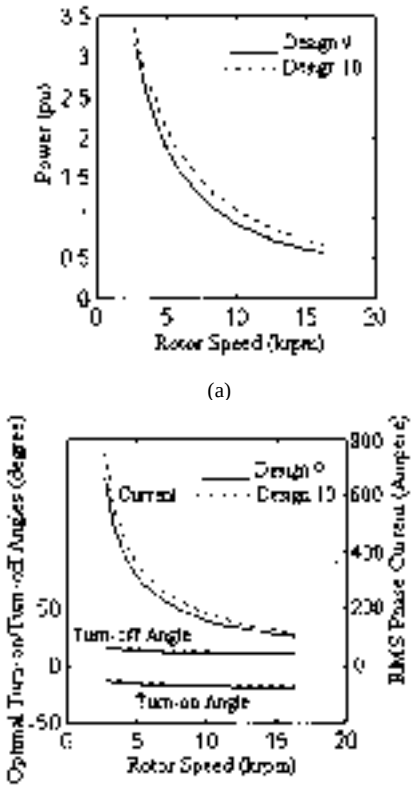

Fig. 18. (a) Maximum overload power and (b) rms phase current and optimal angles for SRM designs 9 and 10.

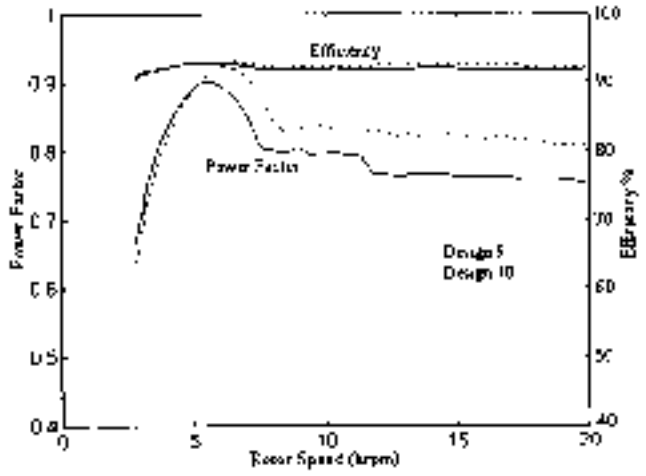

Fig. 17. Efficiency and PF of motors 9 and 10 for the maximum power output.

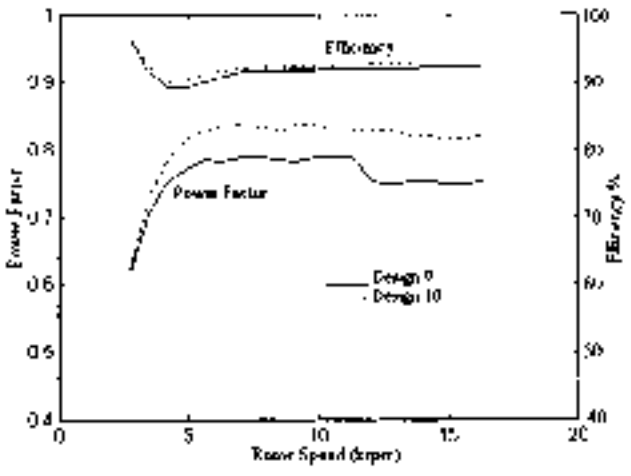

Fig. 19. Efficiency and PF of motors 9 and 10 during overloading condition.

Finally, in Fig. 18 we show the overload capabilities of these designs. The PF's and efficiencies for the overloaded operation are shown in Fig. 19. Design 10 has better PF, better efficiency, and also better overload capability. Due to the higher unaligned inductance, the overload capability of the 8-6 designs are, however, lower than the 6-4 designs.

In this section, we have presented eight 6-4 SRM designs and two 8-6 SRM designs. The 6-4 designs are showing much longer constant power capability and much higher overload capability than the 8-6 designs. The 8-6 designs, however, have higher rated torque and power. They also exhibit better PF and efficiency. A valid comparison between these designs can only be made if we compare the vehicle performance, e.g., the initial acceleration performance, when these motors are used as the propulsion system. This comparison will be made in the next section.

TABLE I
MOTOR POWER RATINGS AND VEHICLE ACCELERATION TIME

SRM Design #	Accl. time (s)	SRM Power (kW)	SRM KVA	IM Power (KW)	IM KVA	BLDC Power (KW)	BLDC KVA
1	13	42.1	69.8	57.88	72.35	75.5	83.9
2	13.25	42.56	69.86	56.9	71.13	74.43	82.7
3	13.48	42.61	69.9	56	70	73.27	81.41
4	13.58	45.88	69.85	55.68	69.6	72.78	80.86
5	13.85	39.1	64.76	54.7	68.38	71.46	79.4
6	14.78	34.6	59.35	51.68	64.6	67.39	74.88
7	14.1	38.98	64.68	53.85	67.3	70.34	78.15
8	15.41	35.38	59.32	50.1	62.6	66.4	73.77
9	16.1	68.12	101.4	72.7	90.88	95.67	106.3
10	8.74	69.95	109.3	83.04	103.8	109.6	121.8

VII. VEHICLE PERFORMANCE ANALYSIS

In this section, we will compare the performance of the designed SRM's for a vehicle propulsion system by calculating the 0–60-mi/h acceleration time. The SRM performance will also be compared with the performance of an induction motor (IM) and a brushless dc (BLDC) motor. For the later comparison, we will calculate the power and the input voltampere requirements of an IM and a BLDC motor for the 0–60-mi/h acceleration in times specified by the SRM's. For this purpose, we consider the following vehicle:

- vehicle rated speed of 26.82 m/s (60 mi/h);
- vehicle maximum speed of 44.7 m/s (100 mi/h);
- vehicle mass of 1450 kg;
- rolling resistance coefficient of 0.013;
- aerodynamic drag coefficient of 0.29;
- frontal area of 2.13 m^2;
- wheel radius of 0.2794 m (11 in);
- level ground;
- zero head wind.

For calculating the acceleration time, the maximum power capabilities of SRM's, presented in Figs. 4, 10, and 16, will be assumed. For calculating the IM power and voltampere, we will assume a constant-power capability of four times the base speed and a PF of 0.8. While, a constant-power range of 2.2 times the base speed and a PF of 0.9 will be assumed for the BLDC motor.

Table I lists the 0–60-mi/h acceleration time, power, and input kilovoltampere ratings of the IM, BLDC motor, and SRM's.

Among the 6-4 designs, design 1, which has the narrowest rotor poles, requires the least amount of time for the acceleration. Design 6, which has the longest constant power range, is requiring longer time for the initial acceleration due to its lower power rating. The 8-6 designs have a much higher power rating than the 6-4 designs, the acceleration time is, therefore, much lower for the 8-6 designs, despite their relatively lower constant power range. The 6-4 SRM's have better overload capability than the 8-6 designs. They also operate in a lower level of saturation. Their performance, therefore, can be improved significantly by increasing the current density. However, more efficient cooling of the motor would be required. The rotor pole height of designs 1–4 can also be reduced to make more room for phase windings. This will, however, increase the unaligned inductance

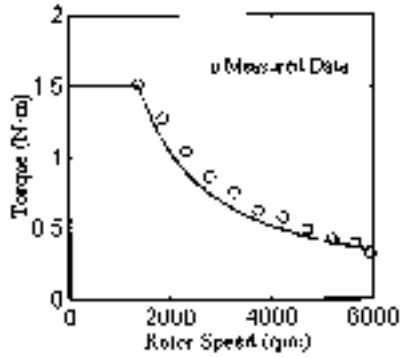

(a)

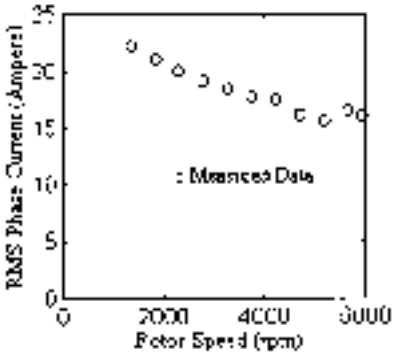

(b)

Fig. 20 (a) Experimentally measured torque and (b) rms phase current at high speed.

and, consequently, the constant-power range, the overload capability, as well as the PF will be reduced. SRM's are exhibiting equal or better performance than the induction and BLDC motors. Of course, a more valid comparison should also include the volume and the weight of the motors. This is, however, beyond the scope of this paper.

VIII. EXPERIMENTAL RESULTS

SRM designs presented inSection VI show that an extremely long constant-power range is possible if the motor is designed appropriately and controlled optimally. A range of three to seven times the base speed has been demonstrated with different designs. In this section, we will present experimental results to demonstrate that an extended constant-power range is possible from the SRM. The experimental motor, however, is a small motor available commercially. The motor was not designed specifically following the methodology presented in this paper. However, it will be controlled with the optimal control parameters. The optimal control parameters are calculated from the dynamic model. The nonlinear field solutions for this motor are calculated from the experimentally collected data. Simulation results for this motor show that an extended range exceeding 6.5 times the base speed is possible. Detailed simulations results of this motor can be obtained in [16].

Fig. 20 shows the experimentally measured torque and rms phase current at high speed when the motor is controlled optimally. The experimental setup has a maximum speed limitation of 6000 r/min. Therefore, we limited our experiment to 6000 r/min. The measured constant-power range is almost 4.35 times

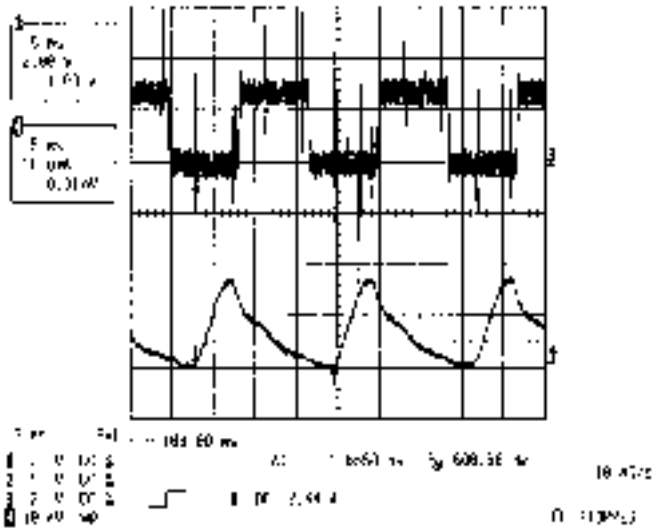

Fig. 21 Actual (lower trace) and the commanded (upper trace) current at 6000 r/min. The oscilloscope scales are 21 and 20 A per division for the commanded and the actual current, respectively.

the base speed. There is still some room available for phase advancing. This can be seen from the phase current waveform near 6000 r/min (Fig. 21). The measured rms phase current decreases while maintaining constant power, indicating, as predicted theoretically, an improvement in the PF.

IX. Conclusion

High-speed capabilities of several 6-4 and 8-6 designs have been presented in this paper. Simulation results show some interesting characteristics of the SRM. Extremely long constant-power ranges are available from the 6-4 designs. PF improves significantly at the high speeds from its low-speed values. Almost 40% more than the design rated power is obtained at high speed without exceeding the voltage and the current ratings of the motors. Excellent efficiencies are exhibited by these designs at high speed. The design examples presented in this paper by no means are the best design geometries. Nevertheless, a design methodology is presented and the potential of the SRM for vehicle application is clearly demonstrated. The SRM definitely shows the potential for performance superior to BLDC's and IM's. A constant-power range of more than four times the base speed is demonstrated by the 8-6 experiment motor. The experimental results also demonstrate the improvement of PF at the high-speed operation.

References

[1] P. J. Blake, R. M. Davis, W. F. Ray, N. N. Fulton, P. J. Lawrenson, and J. M. Stefenson, "The control of switched reluctance motors for battery electric road vehicles," in *Proc. Int. Conf. PEVD*, May 1984, pp. 361–364.

[2] J. H. Lang and F. J. Vallese, "Variable reluctance motor drives for electric propulsion," U.S. Department of Energy, Washington, DC, Rep. DOE/CS-54209-26, May 1, 1985.

[3] J. Corda and J. M. Stephenson, "Analytical estimation of the minimum and maximum inductances of a doubly-salient motor," in *Proc. Int. Conf. Stepping Motors and Systems*, 1979, pp. 50–59.

[4] T. Uematsu and R. S. Wallace, "Design of a 100 kW switched reluctance motor for electric vehicle propulsion," in *Proc. IEEE APEC*, 1995, pp. 411–415.

[5] M. Ehsani, K. M. Rahman, and H. Toliyat, "Propulsion system design of electric and hybrid vehicles," *IEEE Trans.Ind. Electron.*, vol. 44, pp. 7–13, Feb. 1997.

[6] J. V. Byrne and J. B. O'dwyer, "Saturable variable reluctance machine simulation using exponential functions," in *Proc. Int. Conf. Stepping Motors and Systems*. Leeds, U.K., 1976, pp. 11–16.

[7] T. J. E. Miller and M. McGlip, "Nonlinear theory of switched reluctance motor for rapid computer-aided design," *Proc. Inst. Elect. Eng.*, pt. B, vol. 137, no. 6, pp. 337–347, Nov. 1990.

[8] D. A. Torrey, X.-M. Niu, and E. J. Unkauf, "Analytical modeling of variable-reluctance machine magnetization characteristics," *Proc. Inst. Elect. Eng.—Elect. Power Applicat.*, vol. 142, no. 1, pp. 14–22, Jan. 1995.

[9] T. J. E. Miller, *Switched Reluctance Motor and Their Control*. London, U.K.: Clarendon, 1993.

[10] K. M. Rahman, A. V. Rajarathnam, and M. Ehsani, "Optimized instantaneous torque control of switched reluctance motor by neural network," in *Conf. Rec. IEEE-IAS Annu. Meeting*, New Orleans, LA, Oct. 1997, pp. 556–563.

[11] I. Husain, K. R. Ramani, and M. Ehsani, "Torque ripple minimization in switched reluctance motor drives by PWM current control," *IEEE Trans. Power Electron.*, vol. 11, pp. 83–88, Jan. 1996.

[12] A. Ralston and P. Rabinowitz, *A First Course in Numerical Analysis*. New York: McGraw-Hill, 1978.

[13] T. J. E. Miller, *Brushless Permanent-Magnet and Reluctance Motor Drives*. Oxford, U.K.: Oxford Science, 1989.

[14] W. L. Soong and T. J. E. Miller, "Field weakening performance of brushless synchronous AC motor drives," *Proc. Inst. Elect. Eng.—Elect. Power Applicat.*, vol. 141, no. 6, pp. 331–340, Nov. 1994.

[15] P. N. Materu and R. Krishnan, "Estimation of switched reluctance motor losses," *IEEE Trans. Ind. Applicat.*, vol. 28, pp. 668–679, May/June 1992.

[16] K. M. Rahman, G. Suresh, B. Fahimi, A. V. Rajarathnam, and M. Ehsani, "Optimized torque control of switched reluctance motor at all operational regimes using neural network," in *Conf. Rec. IEEE-IAS Annu. Meeting*, St. Louis, MO, 1998, pp. 701–708.

Khwaja M. Rahman (S'94–M'98) received the B.Sc. and M.Sc. degrees from Bangladesh University of Engineering and Technology, Dhaka, Bangladesh, in 1987 and 1990, respectively, and the M.S. and Ph.D. degrees from Texas A&M University, College Station, in 1992 and 1998, respectively, all in electrical engineering.

From 1987 to 1990, he was with the Electrical Engineering Department, Bangladesh University of Engineering and Technology, as a Lecturer. In 1998, he joined General Motors Advanced Technology Vehicles, Torrance, CA, as a Research Engineer. His research interests include variable-speed motor drives and motor drives design and control for electric and hybrid electric vehicles.

Babak Fahimi (S'96–M'99) received the B.S. and M.S. degrees in electrical engineering from Tehran University, Tehran, Iran, in 1991 and 1993, respectively, and the Ph.D. degree in electrical engineering from Texas A&M University, College Station, in 1999.

From August 1993 to September 1995, he was a DAAD Scholar at the Institute for Electric Machines, Aachen, Germany. Currently, he is a Postdoctoral Associate in the Department of Electrical Engineering, Texas A&M University, involved in design and control of electric motor drives for traction applications, application of advanced motor drives in automotive industry, and noise and vibration in electric machinery.

G. Suresh (S'95) received the B.E. degree in 1989 from Annamalai University, Annamalai Nagar, India, and the M.S. degree in 1992 from the Indian Institute of Technology, Madras, India, both in electrical engineering. He is currently working toward the Ph.D. degree in electrical engineering at Texas A&M University, College Station.

From June 1992 to August 1995, he was a Senior Engineer in the Research and Development Department, Kirloskar Electric Company, Bangalore, India. His research interests include electrical machines, power electronics, and microcomputer applications in control of switched reluctance and induction motor drives.

Anandan Velayutham Rajarathnam (S'95) received the B.Eng. degree in electrical and electronics engineering from Coimbatore Institute of Technology, Coimbatore, India, in 1992. He is currently working toward the Ph.D. degree in electrical engineering at Texas A&M University, College Station.

For a year following receipt of the B. Eng. degree, he was with Southern Petrochemical Industries Corporation, Madras, India, as an Engineering Management Trainee, involved in the study of industrial variable-speed motor drives and captive power generation and distribution. His research interests include power electronics, variable-speed drives and digital applications in control and sensorless operation of electric drives.

Mr. Rajarathnam is a student member of the IEEE Industry Applications and IEEE Power Electronics Societies.

M. Ehsani (S'73–M'75–SM'84–F'96) received the Ph.D. degree in electrical engineering from the University of Wisconsin, Madison, in 1981.

Since 1981, he has been with Texas A&M University, College Station, where he is currently a Professor of Electrical Engineering and Director of the Texas Applied Power Electronics Center (TAPC). He is the author of more than 180 publications on pulsed-power supplies, high-voltage engineering, power electronics and motor drives. In 1992, he was named the Halliburton Professor in the College of Engineering, Texas A&M University. In 1994, he was also named the Dresser Industries Professor in the same college. He is the coauthor of a book on converter circuits for superconductive magnetic energy storage and a contributor to the *IEEE Guide for Self-Commutated Converters* and other monographs. He is the holder of thirteen U.S. and EC patents. His current research work is in power electronics, motor drives, hybrid electric vehicles and systems.

Prof. Ehsani has been a member of the IEEE Power Electronics Society AdCom, Past Chairman of the PELS Educational Affairs Committee, Past Chairman of the IEEE Industry Applications Society Industrial Power Converter Committee, and Past Chairman of the IEEE Myron Zucker Student-Faculty Grant Program. He was the General Chair of the IEEE Power Electronics Specialist Conference for 1990. He is an IEEE Industrial Electronics Society Distinguished Speaker and IEEE Industry Applications Society Distinguished Lecturer. He was the recipient of the Prize Paper Award in Static Power Converters and Motor Drives at the IEEE Industry Applications Society 1985, 1987, and 1992 Annual Meetings. He is also a Registered Professional Engineer in the State of Texas.